ELSEVIER

International Journal of Solids and Structures 41 (2004) 3545–3564

INTERNATIONAL JOURNAL OF SOLIDS and STRUCTURES

www.elsevier.com/locate/ijsolstr

A new model for the elastoplastic characterization and the stress–strain determination on the necking section of a tensile specimen

Giuseppe Mirone *

Facolta di Ingegneria di Catania, Department of Mechanical and Industrial Engineering, University of Catania, Viale Andrea Doria 19, 95125 Catania, Italy

Received 22 July 2003; received in revised form 26 January 2004
Available online 19 March 2004

Abstract

The static elastoplastic characterization of metals consists of the determination, by way of experimental tensile tests, of the curve expressing the equivalent von Mises stress as a function of the equivalent plastic strain for each given material. For ductile metals capable of undergoing large post-necking deformations, the knowledge of the stress and strain distributions on the necked cross-section of the tensile specimens is essential for the above characterization. The most known and used solution of the necking problem, due to Bridgman, leads to material curves affected by an error ranging from few percentages up to more than 10% and requires a significant amount of experimental work in order to measure the evolving curvature radius of the necking profile at different stages of each tensile test.

According to many experimental and numerical observations, carried out in previous works and reported also in the present one, the perturbing effect of the necking phenomenon on the stress and strain distributions has been found to be almost material-independent, the only material-dependence consisting of the plastic strain value which triggers the whole necking initiation. The material-independence of the necking effect has been evidenced on a wide set of materials ranging from low and mild steel to inoxidable steel, spheroidized steel, aluminium, copper.

Based on these considerations, a new material-independent solution of the necking problem is finally derived, achieving an error level less than half that obtainable with the Bridgman method. The developed method is very simple to be used because does not require the experimental efforts intrinsic in the use of the Bridgman method.

Keywords: Necking; Plasticity; Stress–strain curve

1. Introduction and basis of the model

The stress–strain characterization of elastoplastic metals consists of the experimental determination of the relationship $\sigma_{eq}(\varepsilon_{eq})$ which returns the von Mises equivalent stress as a function of the equivalent plastic strain.

* Tel.: +39-95-7382418; fax: +39-95-330258.
E-mail address: gmirone@diim.unict.it (G. Mirone).

0020-7683/$ - see front matter © 2004 Elsevier Ltd. All rights reserved.
doi:10.1016/j.ijsolstr.2004.02.011

By definition, these two variables are expressed as follows:

$$\sigma_{\mathrm{eq}} = \sqrt{\frac{3}{2}[\sigma_z'^2 + \sigma_r'^2 + \sigma_\vartheta'^2]} \tag{1}$$

$$\dot{\varepsilon}_{\mathrm{eq}} = \sqrt{\frac{2}{3}[\dot{\varepsilon}_z^2 + \dot{\varepsilon}_r^2 + \dot{\varepsilon}_\vartheta^2]} \tag{2}$$

The terms σ_i' and ε_i in Eqs. (1) and (2) are respectively the deviatoric components of the stress tensor and the components of the plastic strain tensor, both referred to the principal coordinate system.

The experimental data needed to apply (1) and (2) could be obtained, in principle, by pulling tensile specimens with either circular or rectangular cross-section, however the round bar specimens are usually preferred; in fact, at large plastic strains, the rectangular cross-section is subjected to a "non-proportional" area reduction which makes difficult the experimental measurement of the current resisting area. A method to overcome this problem has been proposed by Zhang et al. (1999), consisting of a normalization procedure which predicts the total area reduction as a function of the thickness reduction and of the non-proportional area reduction calculated at a single specific strain level.

In case of axial symmetry, typical of the round bar specimens treated in this work, the principal stress directions are axial (z), radial (r), and circumferential (θ), and when the strain rates are low enough to not influence the material behavior, Eq. (2) applies also without time derivatives.

Tensile tests performed on cylindrical specimens allow to easily derive the equivalent stress and the equivalent plastic strain during the pre-necking phase of the material life, while the specimen experiences just uniform straining; in fact, in these conditions, the stress state is uniform and uniaxial all over the specimen volume, thus the equivalent stress and the equivalent plastic strain can be calculated as in Eqs. (3) and (4) respectively:

$$\sigma_{\mathrm{eq}} = \sigma_z = \sigma_{z\mathrm{Avg}} = \frac{L}{\pi \cdot a^2} \tag{3}$$

$$\varepsilon_{\mathrm{eq}} = \varepsilon_z = \varepsilon_{z\mathrm{Avg}} = 2 \cdot \mathrm{Ln}\left(\frac{a_0}{a}\right) \tag{4}$$

where the current load L, the current cross-section outer radius a and the initial cross-section outer radius a_0 can be easily measured by experiments. The points of coordinates $(\sigma_{\mathrm{eq}}, \varepsilon_{\mathrm{eq}})$ obtained with the mentioned measurements at different time intervals during the test, from the beginning up to the specimen failure, are usually approximated by way of curves having the form of Eq. (5):

$$\sigma_{\mathrm{eq}}(\varepsilon_{\mathrm{eq}}) = K \cdot \varepsilon_{\mathrm{eq}}^{\varepsilon_{\mathrm{N}}} \tag{5}$$

where ε_{N} is the Considère strain (the strain value at which, for the given material, the load starts to decrease and the necking initiates) and the constant K is determined by way of fitting techniques such as the least squares method.

The curve so obtained, usually identified as the "true-stress (σ_{true}) true-strain ($\varepsilon_{\mathrm{true}}$) curve" or briefly as the "true curve", characterizes correctly the material only in the pre-necking phase of the straining; during the post-necking phase this curve differs substantially from the real material curve $\sigma_{\mathrm{eq}}(\varepsilon_{\mathrm{eq}})$ because, since the necking phenomenon arises, the stress state departs gradually from uniaxiality (radial and hoop stresses do not vanish anymore) and from uniformity across the neck section (all the principal stress distributions exhibit a maximum at the center of the neck section and decrease toward the section boundaries).

Summarizing, the true-stress (current ratio between load and resisting area) is perfectly coincident with the local axial stress and with the local von Mises stress on the neck center only until the necking initiates, on the contrary, under well-developed necking conditions, these three stresses differ substantially each other. Fig. 1 clarifies, qualitatively, the necking-induced differences between the true curve and the

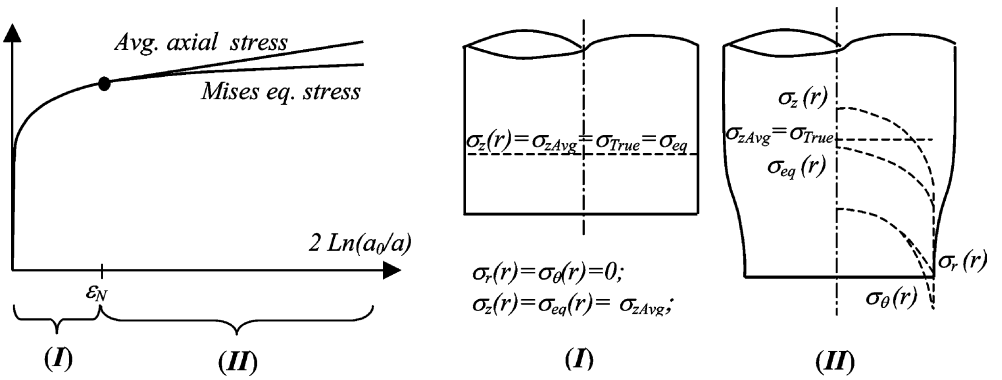

Fig. 1. Difference in the post-necking phase between the true curve and the real material curve.

equivalent-stress vs. equivalent-strain curve, the latter being not experimentally determinable but, at the same time, the only one able to characterize the elastoplastic behavior of a metal.

From the above considerations derives that the true curve is termed true more for conventional reasons than for its effective properties.

The most used method to evaluate the von Mises equivalent stress from experimental data is due to Bridgman (1956), and is capable of estimations whose error has been found to vary between 3% and 13% (Earl and Brown, 1976; Alves and Jones, 1999; La Rosa et al., 2000a,b, 2003). A slightly different approach to the solution of the necking problem was attempted by Earl and Brown (1976), but also in this case the core of the model was the approximate equilibrium equation proposed by Bridgman.

All these methods require the experimental measurement of triplets of the kind (L, a, R) at different instants of the tensile test, in order to return, at the same instants, couples $(\sigma_{\mathrm{eq}}, \varepsilon_{\mathrm{eq}})$ which are estimated points of the constitutive curve. Many points of this kind are usually fitted in order to obtain the material curve in the form of the function $\sigma_{\mathrm{eq}}(\varepsilon_{\mathrm{eq}})$.

The variables L and a constitute the basic experimental measurements usually performed for the determination of the true curve, but R, which is the current curvature radius of the necking profile, is only needed to apply the Bridgman method and is quite difficult to be measured. In fact it requires techniques of image acquisition and analysis to graphically retrieve the necking profiles at different instants of the test, then fitting techniques to approximate the profiles by way of second or third order polynomials, and finally the derivatives of the polynomials may be calculated leading to the desired curvature values R. This procedure, whose final result is the set of equations (6), is very time-consuming and may induce errors up to more than 10%. Furthermore, it predicts an uniform distribution of the equivalent stress and of the three principal strains across the neck section (in the last three equations of (6) does not appear the variable r), while these are known to be non-uniformly distributed as qualitatively depicted in Fig. 1.

$$
\begin{aligned}
&\sigma_z(r) = \sigma_{\mathrm{eq}}\left(1 + \mathrm{Ln}\left[\frac{a^2 - r^2 + 2aR}{2aR}\right]\right)\\
&\sigma_r(r) = \sigma_\vartheta(r) = \sigma_{\mathrm{eq}}\,\mathrm{Ln}\left[\frac{a^2 - r^2 + 2aR}{2aR}\right]\\
&\sigma_{\mathrm{eq}}(\varepsilon_{\mathrm{eq}}) = \sigma_{\mathrm{true}}(\varepsilon_{\mathrm{true}}) \cdot \frac{1}{\left(1 + 2\frac{R}{a}\right) \cdot \mathrm{Ln}\left(1 + \frac{a}{2\cdot R}\right)}\\
&\varepsilon_r(r) = \varepsilon_\vartheta(r) = -\mathrm{Ln}(a_0/a)\\
&\varepsilon_{\mathrm{eq}}(r) = \varepsilon_z(r) = \varepsilon_z = 2\,\mathrm{Ln}(a_0/a) \quad \text{for each } r \in [0, a]
\end{aligned}
\tag{6}
$$

The new method proposed in this work for the elastoplastic characterization of materials derives from some considerations reported in the literature with regard to the R/a parameter and to the true stress/flow stress ratio.

Many experimental values of R/a were evaluated in the Bridgman work, for various steels, bronze and brass, then plotted against the logarithmic plastic strain, obtaining a band of points which departs from the mean line within about 25%, suggesting the possible independency of R/a from the material considered. In the same work, Bridgman makes the hypothesis that "... R/a is the same function of the extension for all steels..." and successively presents also a plot showing the ratio of the flow stress to the true-stress which should apply to round specimens made of every ductile metal.

Also Hill (1950) reports an empirical formula approximating the R/a ratio as a function of the logarithmic plastic strain, referring generally to an elastic–plastic material, and in the work from Saie et al. (1982), a linear law is proposed to approximate the experimental values of R/a with a linear function of the difference $\varepsilon_{eq} - \varepsilon_N$ between the current equivalent strain and the Considère strain.

According to the Bridgman model's equation (6), the ratio R/a completely describes the whole necking effect on the stress and strain distributions, thus, if its material-independency is assumed, then also the relationship between true-stress and equivalent stress, and more generally the global effect of the necking phenomenon on the stress and strain distributions, are to be regarded as material-independent.

In the opinion of the author, three aspects in the above viewpoint could be revised and improved, namely, the approximations in the Bridgman model regarding the uniformity of the strains and of the flow stress all over the neck section, the adoption of the R/a ratio given by a function which approximates experimental data of difficult and imprecise measurement, and the adoption of just the logarithmic plastic strain as the variable governing the evolution of the necking effect; in fact, the first point is a clear approximation, the second one could induce a considerable error in the material characterization procedure because is based on very difficult measurements, the last one is conceptually wrong because the same amount of total logarithmic strain corresponds to very different post-necking strains depending on the value assumed by the Considère parameter for each material. With regard to the latter aspect, Saie et al. (1982) avoided this error by approximating the R/a ratio as a function of $\varepsilon_{eq} - \varepsilon_N$ rather than just ε_{eq}.

All the Bridgman-based approaches attempted to derive a material-independent relationship between the true-stress and the flow stress passing through the determination of the parameter R/a which is essential to apply the Bridgman method.

To investigate on the necking phenomenon without dealing with the mentioned approximations and with the parameter R/a, tensile tests of cylindrical specimens made of many different metals were experimentally carried out and then simulated by way of finite elements analyses in previous works (La Rosa et al., 2000a,b, 2001, 2003), looking for a relationship between the true-stress (which is the only stress easily measurable by experiments) and the equivalent stress which really expresses the material hardening properties.

These analyses were performed using materials curves derived from experimental true-stress true-strain data, some found in the literature and the others resulting from experiments purposefully carried out.

All the numerical analyses were performed taking into account for the geometric and material nonlinearities by way of the algorithms available with the MARC finite elements code (large displacements, finite strains, isotropic hardening, von Mises plasticity).

The accuracy of each material curve was determined by comparing the experimental data with the FEA results: the material curve to be examined was used to drive a nonlinear FE analysis simulating the tensile test, then a comparison was performed between the true curve predicted in the FE results and the one experimentally determined; if the two true curves were coincident each other, then the material curve used as input for the numerical analysis was the right one to model the elastic–plastic behavior of the considered material.

Once the material curves and the whole FE models were validated by way of the above comparison, many values of the equivalent stress averaged onto the neck section, σ_{eqAvg}, were calculated from the FE results at different integration steps (different strain levels), for each material. At the same integration steps were extracted also the values of the true-stress $\sigma_{z\mathrm{Avg}} = L/(\pi a^2)$ and of the true-strain $\varepsilon_{\mathrm{eqAvg}} \approx \varepsilon_{z\mathrm{Avg}} = 2\,\mathrm{Ln}(a_0/a)$.

Finally, for each material, the ratio $\sigma_{\mathrm{eqAvg}}/\sigma_{z\mathrm{Avg}}$ so determined from the FE results was plotted against the reduced post-necking strain defined as $\varepsilon_{\mathrm{eqAvg}} - \varepsilon_{\mathrm{N}}$. This investigation gave the result visible in Fig. 1, where the materials listed in the legend correspond respectively to inoxidable steel, medium carbon steel, low carbon steel, 2011 aluminium alloy, four different grades of spheroidized steel (experimental true curves from Le Roy et al., 1981), Hysol 130 and Navy Quality 1 steel (experimental true curves from Hancock and Mackenzie, 1976; Mackenzie et al., 1977; Hancock and Brown, 1983; Thomson and Hancock, 1984). Other material curves were tested in the past, and the scattering of the analyzed ratio never exceeded 7% of the average value in every case, with no regard for the great differences exhibited by the material curves investigated. Furthermore it was verified that this scattering depends almost exclusively on the numerical integration step size, so that, decreasing the latter indefinitely, an almost common trend could be obtained for all the materials. The data of Fig. 2 evidences the material-independency of the ratio $\sigma_{\mathrm{eqAvg}}/\sigma_{z\mathrm{Avg}}$, so that a curve able to fit the plotted points promises a maximum error close to half the scattering, thus close to 3%.

The points in Fig. 2 have been approximated by a polynomial named $\mathrm{MLR}_{\sigma}(\varepsilon_{\mathrm{eqAvg}} - \varepsilon_{\mathrm{N}})$ which, due to its definition, is able to transform the experimental true-stress $\sigma_{z\mathrm{Avg}}$ into an estimation of the equivalent stress averaged onto the neck cross-section, σ_{eqAvg}, for virtually all the materials satisfying the von Mises plasticity. The error level is close to 3% as mentioned above (La Rosa et al., 2003), thus the MLR_{σ} function constitutes an approximate material characterization tool more accurate and much easier to be used than the Bridgman method.

These findings induced to suppose that other ratios between neck-averaged stresses and/or strains could show a similar material-independence, so that further investigations were performed in this direction leading to the first new finding presented in this work, namely the ratio between two principal plastic strains averaged onto the neck section, $\varepsilon_{r\mathrm{Avg}}/\varepsilon_{\theta\mathrm{Avg}}$, plotted in Fig. 3 against $\varepsilon_{\mathrm{eq}} - \varepsilon_{\mathrm{N}}$.

The ε_r and ε_θ distributions from which the section-averaged values are obtained, came from finite element analyses similar to those previously described, now referring to the 10 materials listed in the legend.

As in the case of the ratio shown in Fig. 2, also the last one has been fitted with a polynomial, termed $\mathrm{MLR}_{\varepsilon}(\varepsilon_{\mathrm{eqAvg}} - \varepsilon_{\mathrm{N}})$, able to represent the data of Fig. 3 within an error close to 3%.

The two MLR functions depend on the current value of logarithmic plastic strain, $\varepsilon_{\mathrm{eqAvg}} \approx 2\,\mathrm{Ln}(a_0/a)$, and on the value that this strain assumes at necking initiation, ε_{N}, which is a material constant.

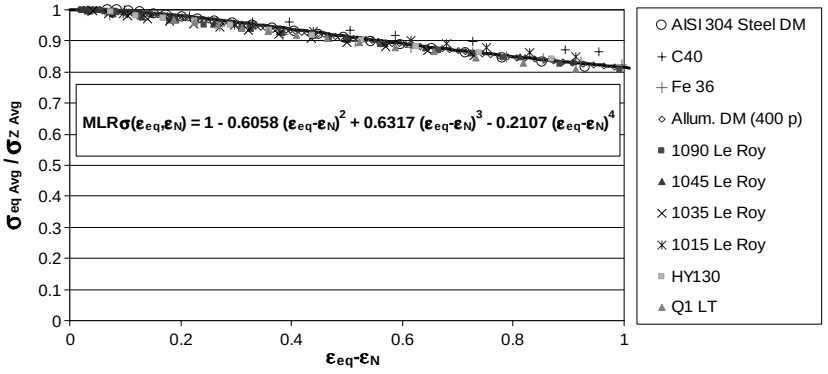

Fig. 2. Ratio $\sigma_{\mathrm{eqAvg}}/\sigma_{z\mathrm{Avg}}$ vs. $\varepsilon_{\mathrm{eqAvg}} - \varepsilon_{\mathrm{N}}$ for different materials.

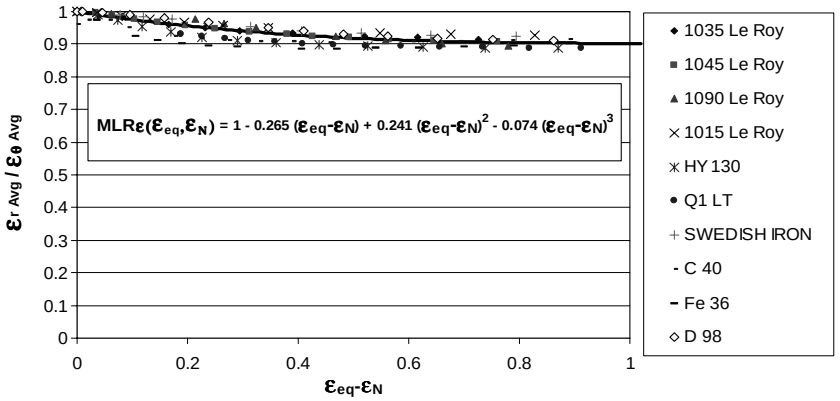

Fig. 3. Ratio $\varepsilon_{r\mathrm{Avg}}/\varepsilon_{t\mathrm{Avg}}$ vs. $\varepsilon_{\mathrm{eqAvg}} - \varepsilon_{\mathrm{N}}$ for different materials.

2. MLR model development—strain distributions

During the post-necking phase, the elastic component of the total strain may be usually neglected because, for typical ductile metals, it is two or three magnitude orders smaller than the plastic strain which is the subject of our investigation.

The knowledge of $\mathrm{MLR}_{\sigma}(\varepsilon_{\mathrm{eqAvg}} - \varepsilon_{\mathrm{N}})$ and $\mathrm{MLR}_{\varepsilon}(\varepsilon_{\mathrm{eqAvg}} - \varepsilon_{\mathrm{N}})$ allows to impose two new mathematical conditions to the set of those usually available for the determination of the stress and plastic strain distributions on the necked section of cylindrical bars.

The first hypothesis introduced here, in order to derive the above distributions, regards the axial plastic strain, $\varepsilon_z(r)$, supposed to be a quadratic functions of the radial abscissa of the neck section r, ranging in the interval $(0, a)$:

$$\varepsilon_z(r) = A + B \cdot r^2 \tag{7}$$

the volume conservation equation imposed on the radial displacement $\rho(r)$ brings:

$$\varepsilon_z(r) + \frac{\rho(r)}{r} + \frac{\partial}{\partial r}(\rho(r)) = 0 \quad \text{with } \frac{\partial}{\partial r}(\rho(r)) = \varepsilon_r(r) \text{ and } \frac{\rho(r)}{r} = \varepsilon_{\vartheta}(r) \tag{8}$$

solving the differential equation derives the displacement equation (9)

$$\rho(r) = \frac{C}{r} - \frac{1}{4}(2A \cdot r + B \cdot r^3) \tag{9}$$

where the integration constant C vanishes because on the specimen axis ($r = 0$), the displacement is null.

Then the radial and hoop strains are respectively:

$$\varepsilon_r(r) = \frac{1}{4}(-2A - 3Br^2) \tag{10}$$

$$\varepsilon_{\vartheta}(r) = \frac{1}{4}(-2A - Br^2) \tag{11}$$

At this stage, the strain state on the necking section is completely described by the two constants A and B.

The first one of these may be calculated imposing that the neck-averaged value of the axial plastic strain must be equal, by definition, to the logarithmic plastic strain:

$$\varepsilon_{z\mathrm{Avg}} = \frac{1}{\pi \cdot a^2} \cdot \int_0^a \varepsilon_z(r) \cdot 2\pi r \cdot \mathrm{d}r = 2\,\mathrm{Ln}\left(\frac{a_0}{a}\right) \Rightarrow A = \frac{1}{2}\left[4\,\mathrm{Ln}\left(\frac{a_0}{a}\right) - B \cdot a^2\right] \tag{12}$$

Substituting (12) in (7), (10) and (11), the principal plastic strains became:

$$\begin{aligned}
\varepsilon_z(r) &= 2\,\mathrm{Ln}\left[\frac{a_0}{a}\right] - B\left[\frac{a^2}{2} - r^2\right] \\
\varepsilon_r(r) &= -\mathrm{Ln}\left[\frac{a_0}{a}\right] + \frac{B}{4}[a^2 - 3 \cdot r^2] \\
\varepsilon_\vartheta(r) &= -\mathrm{Ln}\left[\frac{a_0}{a}\right] + \frac{B}{4}[a^2 - r^2]
\end{aligned} \tag{13}$$

Now the last remaining constant, B, may be determined imposing the new condition found for the average values of the radial and hoop plastic strains:

$$\frac{\varepsilon_{r\mathrm{Avg}}}{\varepsilon_{\vartheta Avg}} = \frac{\dfrac{1}{\pi \cdot a^2}\displaystyle\int_0^a \varepsilon_r(r) \cdot 2\pi \cdot r \cdot \mathrm{d}r}{\dfrac{1}{\pi \cdot a^2}\displaystyle\int_0^a \varepsilon_\vartheta(r) \cdot 2\pi \cdot r \cdot \mathrm{d}r} = \frac{\displaystyle\int_0^a \left[-\mathrm{Ln}\left[\frac{a_0}{a}\right] + \frac{B}{4}(a^2 - 3r^2)\right] \cdot 2\pi \cdot r \cdot \mathrm{d}r}{\displaystyle\int_0^a \left[-Ln\left[\frac{a_0}{a}\right] + \frac{B}{4}(a^2 - r^2)\right] \cdot 2\pi \cdot r \cdot \mathrm{d}r} = \mathrm{MLR}_\varepsilon(a_0, a, \varepsilon_\mathrm{N});$$

$$\Downarrow$$

$$B = \mathrm{Ln}\left(\frac{a_0}{a}\right) \cdot \frac{8}{a^2} \cdot \frac{(\mathrm{MLR}_\varepsilon(a_0, a, \varepsilon_\mathrm{N}) - 1)}{(\mathrm{MLR}_\varepsilon(a_0, a, \varepsilon_\mathrm{N}) + 1)} \tag{14}$$

The distributions of the three principal plastic strains finally become:

$$\begin{aligned}
\varepsilon_z(r) &= 2 \cdot \mathrm{Ln}\left(\frac{a_0}{a}\right) \cdot \frac{[4r^2 \cdot (\mathrm{MLR}_\varepsilon(a_0, a, \varepsilon_\mathrm{N}) - 1) - a^2 \cdot (\mathrm{MLR}_\varepsilon(a_0, a, \varepsilon_\mathrm{N}) - 3)]}{a^2 \cdot (\mathrm{MLR}_\varepsilon(a_0, a, \varepsilon_\mathrm{N}) + 1)} \\
\varepsilon_r(r) &= -\mathrm{Ln}\left(\frac{a_0}{a}\right) \cdot \frac{[6r^2 \cdot (\mathrm{MLR}_\varepsilon(a_0, a, \varepsilon_\mathrm{N}) - 1) - a^2 \cdot (\mathrm{MLR}_\varepsilon(a_0, a, \varepsilon_\mathrm{N}) - 3)]}{a^2 \cdot (\mathrm{MLR}_\varepsilon(a_0, a, \varepsilon_\mathrm{N}) + 1)} \\
\varepsilon_\vartheta(r) &= -\mathrm{Ln}\left(\frac{a_0}{a}\right) \cdot \frac{[2r^2 \cdot (\mathrm{MLR}_\varepsilon(a_0, a, \varepsilon_\mathrm{N}) - 1) - a^2 \cdot (\mathrm{MLR}_\varepsilon(a_0, a, \varepsilon_\mathrm{N}) - 3)]}{a^2 \cdot (\mathrm{MLR}_\varepsilon(a_0, a, \varepsilon_\mathrm{N}) + 1)}
\end{aligned} \tag{15}$$

A first important consideration which derives from this first part of the model is that, in the plastic strain distributions of Eq. (15), the only material-dependence is represented by the necking initiation strain ε_N. This means that, for the cylindrical geometry considered, the start and the increase of the strain disuniformity across the section, which constitutes the whole perturbing effect of the necking phenomenon, depends only on the amount of post-necking strain cumulated, with no regard for other aspects of the material behavior.

It is possible to say that the shape of the strain distributions and the amount of their non-uniformity depend only on the current value of the reduced strain $\varepsilon_{\mathrm{eqAvg}} - \varepsilon_\mathrm{N}$, while the scale factor of these distributions depends on the total value of the current strain $\varepsilon_{\mathrm{eqAvg}}$.

These findings confirm that the necking could be considered as an instability phenomenon somehow similar to the compressive buckling: in fact, also in the latter case, the Euler critical load for a given geometry strongly depends on a material constant such as the elastic modulus (this triggering role being played by ε_N for the necking), but, once the instability initiates, the shape of the strain distributions are not expected to depend on any material property.

The equivalent plastic strain, according to the proposed approximations, becomes:

$$\varepsilon_{\mathrm{eq}}(r)=\sqrt{\frac{2}{3}\cdot\frac{2\left[\mathrm{Ln}\left(\frac{a_0}{a}\right)\right]^2}{a^4\cdot(\mathrm{MLR}_\varepsilon(a_0,a,\varepsilon_\mathrm{N})+1)^2}\cdot\left[\begin{array}{l}3\cdot a^4\cdot(\mathrm{MLR}_\varepsilon(a_0,a,\varepsilon_\mathrm{N})-3)\\ +24\cdot a^2r^2\cdot\left(\begin{array}{l}-3+4\,\mathrm{MLR}_\varepsilon(a_0,a,\varepsilon_\mathrm{N})\\ -[\mathrm{MLR}_\varepsilon(a_0,a,\varepsilon_\mathrm{N})]^2\end{array}\right)+52\cdot r^4\cdot(\mathrm{MLR}_\varepsilon(a_0,a,\varepsilon_\mathrm{N})-1)\end{array}\right]}. \tag{16}$$

3. MLR model development—stress distributions

Once the plastic strains are determined, the deviatoric stresses may be derived from the incremental plasticity equations as in (17):

$$\begin{aligned}\sigma'_z(r)&=\frac{2}{3}\sigma_{\mathrm{eq}}(r)\cdot\frac{\mathrm{d}\varepsilon_z(r)}{\mathrm{d}\varepsilon_{\mathrm{eq}}(r)}\\ \sigma'_r(r)&=\frac{2}{3}\sigma_{\mathrm{eq}}(r)\cdot\frac{\mathrm{d}\varepsilon_r(r)}{\mathrm{d}\varepsilon_{\mathrm{eq}}(r)}\\ \sigma'_\vartheta(r)&=\frac{2}{3}\sigma_{\mathrm{eq}}(r)\cdot\frac{\mathrm{d}\varepsilon_\vartheta(r)}{\mathrm{d}\varepsilon_{\mathrm{eq}}(r)}\end{aligned} \tag{17}$$

The derivatives appearing at the end of each deviatoric stress have been evaluated referring to the time-like variable a which is the simplest variable, common to all the strains, univocally expressing the whole strain level.

$$\begin{aligned}\frac{\mathrm{d}\varepsilon_z(r)}{\mathrm{d}\varepsilon_{\mathrm{eq}}(r)}&\approx\frac{\partial\varepsilon_z(r)}{\partial a}\cdot\left(\frac{\partial\varepsilon_{\mathrm{eq}}(r)}{\partial a}\right)^{-1}\\ \frac{\mathrm{d}\varepsilon_r(r)}{\mathrm{d}\varepsilon_{\mathrm{eq}}(r)}&\approx\frac{\partial\varepsilon_r(r)}{\partial a}\cdot\left(\frac{\partial\varepsilon_{\mathrm{eq}}(r)}{\partial a}\right)^{-1}\\ \frac{\mathrm{d}\varepsilon_\vartheta(r)}{\mathrm{d}\varepsilon_{\mathrm{eq}}(r)}&\approx\frac{\partial\varepsilon_\vartheta(r)}{\partial a}\cdot\left(\frac{\partial\varepsilon_{\mathrm{eq}}(r)}{\partial a}\right)^{-1}\end{aligned} \tag{18}$$

It is worth to underline that, before the derivatives are calculated, the function $\mathrm{MLR}_\varepsilon(\varepsilon_{\mathrm{eqAvg}}-\varepsilon_\mathrm{N})$ contained in each strain must be put in explicit form because it depends on the variable a, thus needs to be derived together with the remaining terms of each strain function.

Being $\mathrm{MLR}_\varepsilon(\varepsilon_{\mathrm{eqAvg}}-\varepsilon_\mathrm{N})$ a fourth order polynomial (see Fig. 3), the explicit form of Eq. (17) becomes very long, thus the following part of the model, related to the stress calculation, may be handled almost exclusively in a numerical way using commonly available calculus software.

Recalling the results initially presented, the equivalent stress $\sigma_{\mathrm{eq}}(r)$ in (17) is given by:

$$\sigma_{\mathrm{eq}}(r)=\frac{\mathrm{Load}}{\pi\cdot a^2}\cdot\mathrm{MLR}_\sigma(\varepsilon_{\mathrm{eq}}(r)-\varepsilon_\mathrm{N}) \tag{19}$$

where the MLR_σ function is the fourth order polynomial able to fit the data of Fig. 2, independently of the material considered.

So far, the deviatoric stresses are known for every material as functions of a_0, a, ε_N, and Load, all these parameters being the basic data acquired during each tensile tests for the simple true curve calculation. The

last function to be determined for the achievement of the complete stress state on the necking section is the hydrostatic stress, $\sigma_H(r)$, which is known to be independent of the plastic strains for every material obeying to the von Mises plasticity rules.

A second hypothesis, regarding the shape of the hydrostatic stress distribution, is introduced here by approximating σ_H with a quadratic polynomial of the neck section radial abscissa.

$$\sigma_H(r) = H_0 + H_2 \cdot r^2 \tag{20}$$

Two conditions, respectively stating the axial equilibrium on σ_z and the radial equilibrium on σ_r at the outer surface of the neck section (for $r = a$), are imposed in order to derive the constants $H0$ and $H2$ and identify the function $\sigma_H(r)$:

$$\int_0^a 2\pi \cdot r \cdot (\sigma'_z(r) + \sigma_H(r))\,\mathrm{d}r = \text{Load} \tag{21}$$

$$\sigma_r(a) = \sigma'_r(a) + \sigma_H(a) = 0 \tag{22}$$

Once the last two constant are determined, the complete stress state on the necking section is found.

The described functions and equations have been organized in a numerical algorithm so that the distributions of principal strains and principal stresses across the neck section can be obtained by simply inputting a set of parameters to define the known properties of the material at hand and the post-necking strain level at which the whole distributions are required. The parameters needed are:

- The experimental post-necking true curve in the form of polynomial fitting of the experimental data, typically first or second order polynomials (coefficients $S0$, $S1$, $S2$).
- The value of the necking initiation strain ε_N.
- The initial undeformed cross-section radius of the specimen a_0.
- The current cross-section radius of the specimen a.

Obviously, MLR_σ and MLR_ε are used as known material-independent functions, approximated by the polynomials appearing in Figs. 2 and 3, respectively.

4. Experimental test, FEA and reference for the validation of the MLR model

In order to verify the accuracy of the stress and strain distribution models, a suitable reference against which their predictions could be compared was to be found.

A direct comparison between the estimated local distributions (resulting from the Bridgman or the MLR models) and experiments, was not possible because the local values of strains and stresses in the interior of the neck section cannot be measured. Then, the finite element analysis (FEA) was selected as a useful way to indirectly compare the output of the two above models with the experimental results.

In fact, if the FEA simulating a tensile test was able to reproduce, with acceptable accuracy, the experimental evolution of measurable necking parameters (e.g. current load and minimum cross-section diameter or any combination of them), then it was reasonable to assume that also the stress and strain distributions on the neck section, predicted by the same numerical analyses, were close to the real distributions. So the stress and strain distributions resulting from the experimentally-validated FEA were taken as the reference against which to evaluate the accuracy of the distributions predicted by the MLR and the Bridgman models, respectively.

The flow charts in Fig. 4 clarifies the validation and the comparison procedures carried out in the following sections of the paper.

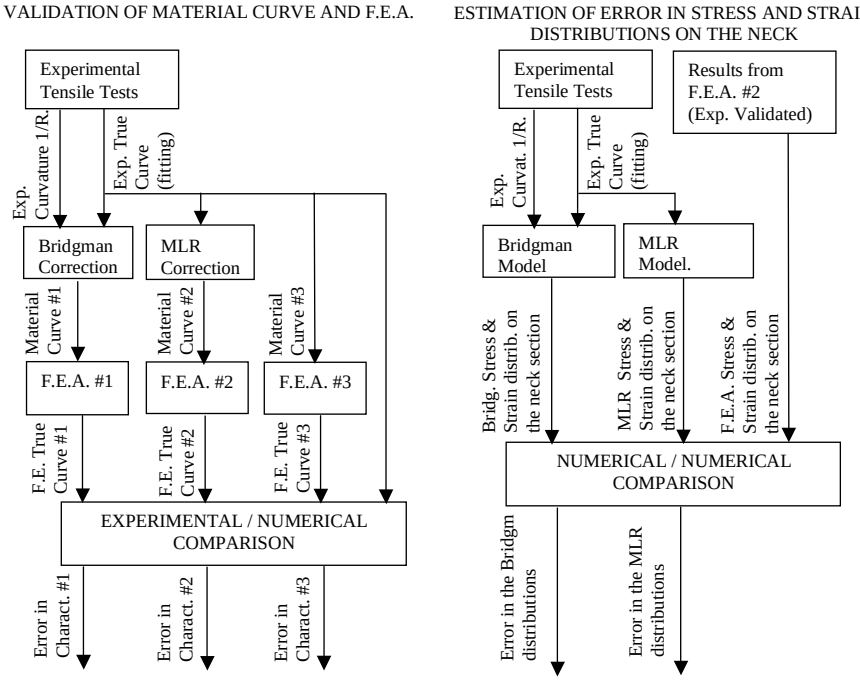

Fig. 4. Validation and comparison flow charts.

Five cylindrical specimens made of 20MnMoNi55 (Fig. 5) have been prepared for the experimental tensile tests.

In order to verify that no strain rate effect was influencing the measured data, specimens were pulled at nominal strain rates ranging from 3×10^{-4} to 1.5×10^{-3}. Values of the current load and close-range images of the necking zone were recorded by way of an Instron 4206 testing machine (20 load values per second) and of a CCD camera connected to a 25 frames per second-frame grabber PC card, respectively. The failure event was used as a timing mark to take, for each tensile test, 20 a posteriori synchronized couples of load values L and images. Then, by way of simple image analysis measurements, the current outer radius a of the neck cross-section was derived from all the selected images, so that 20 couples L, a were available for each pulled specimen. Applying Eqs. (3) and (4) to the latter data, 20 points of the true curve were obtained for every specimen as reported in Fig. 6, where a least squares fitting curve approximating the experimental results is also shown.

The fitting curve in Fig. 6 is given by a power law which applies in the strain range between zero and the necking initiation ε_N (marked with a cross point in Fig. 6), together with a linear law for the strains region beyond ε_N.

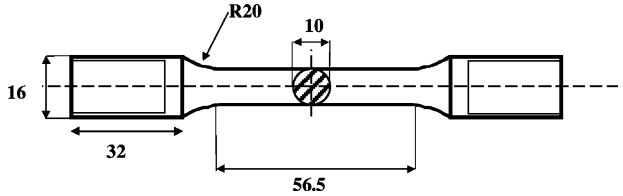

Fig. 5. Specimens geometry.

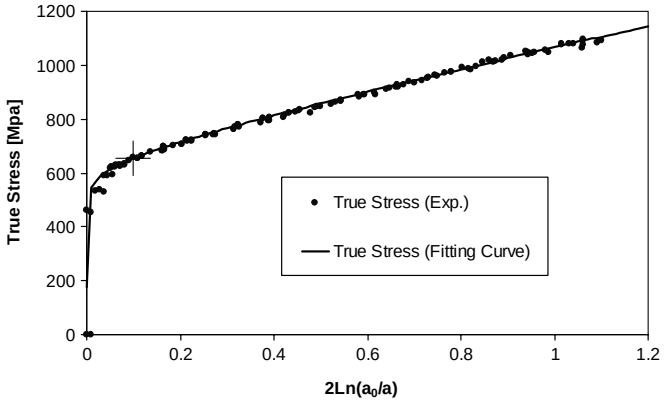

Fig. 6. Experimental results from tensile tests.

The true curve expression as well as other relevant material data, averaged on the results from the entire set of five specimens tested, are reported in Table 1.

Two estimations of the equivalent stress–equivalent strain curve for the tested material were then derived from the above true curve, according to the following description.

The first one, due to Bridgman and performed by way of the third equation in (6), required the knowledge of the necking profile curvature radius R as a function of the logarithmic plastic strain. This was achieved trough profiles detection and analysis on the same neck images previously used for the measurement of the cross-section diameter. To illustrate the curvature measurements, in Fig. 7(a) are reported two necking profiles acquired from specimen #1 at different stages of the test (respectively at $\varepsilon_{eq} = 0.3$ and at incipient failure), while in Fig. 7(b) is shown the evolution of the measured necking curvature radii R during the experimental test of the same specimen.

The two necking profiles of Fig. 7(a) are plotted in pixel units (the length of each pixel being close to 0.05 mm), with the axis origin placed on the intersection point between the necking profile and the neck cross-section; the abscissa of the plot runs parallel to the longitudinal axis of the specimen and each profile divides the plot area in two parts, the upper one corresponding to the specimen body, the lower one corresponding to the background of the image.

Every profile was approximated by a second order polynomial between the two inflection points and successively scaled by assigning the proper length value to each pixel, so that the curvature radius R for each image was easily calculated. To every point of the true curve in the post-necking range was then associated the corresponding Bridgman-estimation of the equivalent stress by multiplying the whole experimental true-stress times the correction factor reported in the third equation of (6). The Bridgman-corrected true-stress values were then approximated by a least square fitting function.

Table 1
Material experimental parameters

		True curve expression	
Elastic modulus, E	200 GPa	$\sigma_{true} = \begin{cases} K \cdot \varepsilon_{true}^{\varepsilon_N} & \text{for } (0 < \varepsilon_{eq} \leqslant \varepsilon_N) \\ S_0 + S_1 \cdot \varepsilon_{true} & \text{for } (\varepsilon_{eq} > \varepsilon_N) \end{cases}$	$K = 828$ MPa
Yield stress, σ_Y	470 MPa		$S0 = 614$ MPa
Necking strain, ε_N	0.1		$S1 = 460$ MPa
Necking stress, σ_N	650 MPa		
Failure strain, ε_F	1.07		

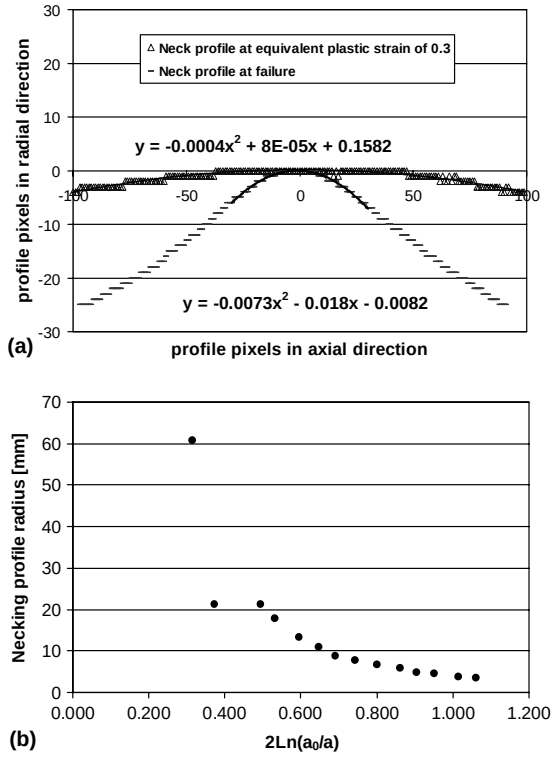

Fig. 7. Experimental necking profiles (a) and curvature radii measurements (b) from specimen #1.

The second estimation of the equivalent stress–equivalent strain curve was obtained, much more easily than in the latter case, by simply multiplying the post-necking true curve times the $\mathrm{MLR}_\sigma(\varepsilon_{eq} - \varepsilon_N)$ function shown in Fig. 2.

Clearly, both the true-stress corrections, respectively from Bridgman and from the MLR_σ function, apply only in the post-necking phase ($\varepsilon_{eq} > \varepsilon_N$) because, for $\varepsilon_{eq} < \varepsilon_N$, the power law approximating the first part of the experimental true curve coincides exactly with the equivalent stress–equivalent strain curve. The two described estimations of the material curve are reported in Fig. 8.

Very small discrepancies between the two evaluations of the material curve are visible in Fig. 8, in fact the maximum difference between them occurs at a strain value close to 0.8, where the Bridgman method predicts an equivalent stress 2.5% higher than the value coming from the new proposed method.

It is worth noting that both the estimations of the material curve predict, at failure, an equivalent stress close to 915 MPa, definitely lower than the true-stress at failure (approximately 1100 MPa). This confirms that, for materials capable of undergoing significant post-necking strains, the difference between the true-stress and the equivalent stress is not negligible; for the tested metal, if the experimental true curve without any correction is taken as the material curve, neglecting the above difference, then a considerable error, close to 20% at failure, is introduced in the material characterization. The analytical expressions of the two post-necking curves of Fig. 8 are reported in Table 2, where the function expressing the Bridgman-estimated equivalent stress is a least square fitting of the Bridgman-corrected experimental true-stress and the pre-necking law is the same reported in Table 1.

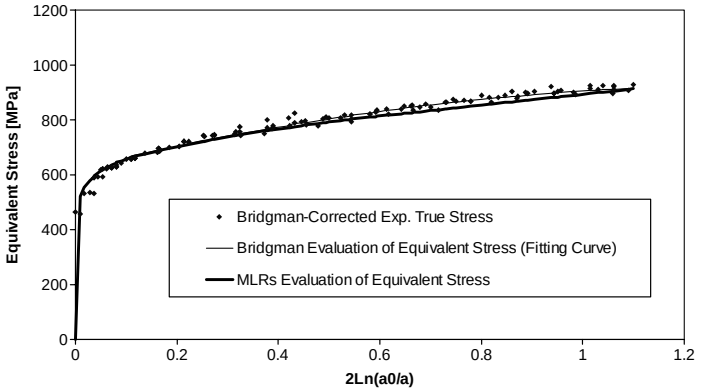

Fig. 8. Different approximations of the equivalent stress–equivalent strain curve.

Table 2
Equations for the estimated relationships between equivalent stress and equivalent strain

Bridgman estimation	$\sigma_{eq} = \begin{cases} K \cdot \varepsilon_{eq}^{\varepsilon_N} & \text{for } (0 < \varepsilon_{eq} \leqslant \varepsilon_N) \\ B_0 + B_1 \cdot \varepsilon_{eq} + B_2 \cdot \varepsilon_{eq}^2 & \text{for } (\varepsilon_{eq} > \varepsilon_N) \end{cases}$	$B_0 = 620$ MPa $B_1 = 450$ MPa $B_2 = -165$ MPa
MLR_σ estimation	$\sigma_{eq} = \begin{cases} K \cdot \varepsilon_{eq}^{\varepsilon_N} & \text{for } (0 < \varepsilon_{eq} \leqslant \varepsilon_N) \\ (S_0 + S_1 \cdot \varepsilon_{iq}) \cdot MLR_\sigma(\varepsilon_{iq} - \varepsilon_N) & \text{for } (\varepsilon_{eq} > \varepsilon_N) \end{cases}$	

So far, we have three possible different curves to characterize the same material:

(i) the Bridgman curve which requires a considerable amount of work to determine the evolution of the necking profile curvature and, for some materials, introduces errors up to 10%; currently it is the most known and widely used in the literature (Le Roy et al., 1981; Saie et al., 1982; Alves and Jones, 1999; Ragab and Saleh, 1999; Zhang et al., 1999; La Rosa et al., 2003);
(ii) the MLR_σ curve, which requires just basic experimental measurements but allows predictions with a precision level equal or higher than the Bridgman curve (La Rosa et al., 2003);
(iii) the experimental true curve without any correction, which requires the same amount of basic experimental data needed for the MLR curve but is known to be inaccurate for strains beyond the necking; despite this, it is frequently used in the literature for materials characterization involving large strains and ductile failure (Needleman and Tvergaard, 1984; Becker et al., 1988; Lemaitre, 1988; Wang, 1992; Chandrakanth and Pandey, 1995; Bonora, 1997).

It is useful to underline that the measurement of many necking profile curvatures, on the same specimen at different instants of its load history, constitutes a considerably difficult task whose precision may vary substantially depending on the digital image resolution adopted, on the distance between specimen and video camera, on the light condition, on the choice of the reasonable length of profile to be approximated by polynomials, etc. These uncertainties might account for a significant part of the approximations which are intrinsic in the use of the Bridgman method.

In order to evaluate the accuracy of the three curves so far determined, the tensile test has been simulated, as described in the first flow chart of Fig. 4, by as many finite element analyses each based on a common model (geometry, boundary conditions, integration steps and algorithms, analysis settings, etc.) coupled, in turn, with all the three constitutive curves to be examined.

The higher is the agreement between a FEA and the experimental results, the greater is the accuracy of the curve assigned to the FE model to define the material.

The common root of the three finite element analyses performed consists of a mesh with 9100 full integration, eight-noded, axisymmetric elements, modeling one-half of the longitudinal section of the cylindrical specimen. One of the two specimen ends is constrained to simulate the fixed clamp of the Instron test machine, on the other end a 12 mm translation, fractioned in 1500 integration steps, is applied in the axial direction to simulate the moving clamp of the machine. The analyses have been performed with the finite displacement, finite strains, updated Lagrangian algorithms available in the MARC code.

The numerical–experimental validation is shown in Fig. 9, where the true-stress resulting from the output of the three finite elements analyses (thus given by the ratio of the current load to the current minimum section area measured on the deformed mesh) are plotted together with the experimental true-stress previously reported in Fig. 6.

Fig. 9 evidences how the experimental true curve, used without any correction to perform the third FE analysis, induces a considerable discrepancy between numerical and experimental true-stress; this error continuously increases during all the post-necking phase, reaching a value close to 20% at failure.

The first FE analysis, in which the Bridgman-estimated flow curve was used as input material curve, exhibits a good performance allowing to reproduce the experimental results with an error lower than 3%.

The second FE analysis, driven by the MLR_{σ}-estimated material curve, gives results closer to the experimental ones than those obtained in the previous case, confirming the findings of other works (La Rosa et al., 2000a,b, 2001, 2003). This evidence, together with the significantly lower amount of experimental work needed for this correction method with respect to the Bridgman method, makes the former approach definitely more advantageous than the latter.

Once the results of the second FE analysis are experimentally validated in terms of macroscopic variables (current values of load and neck diameter combined to give true stresses and strains), becomes reasonable to assume that also the predictions of a more local nature, such as the stress and strain distributions on the neck section, are as well realistic.

The above consideration, together with the impossibility to take experimental measurements in the interior of the necking, leads us to use the distributions from the second FE analysis as the reference for successive validations involving local values of stress and strain on the neck.

Therefore, in the next sections of the paper, the stress and strain distributions on the minimum cross-section calculated by way of the Bridgman method (Eq. (6)) and of the MLR method (equations from (7) to (20)), are compared with the reference distributions predicted by the second FEA.

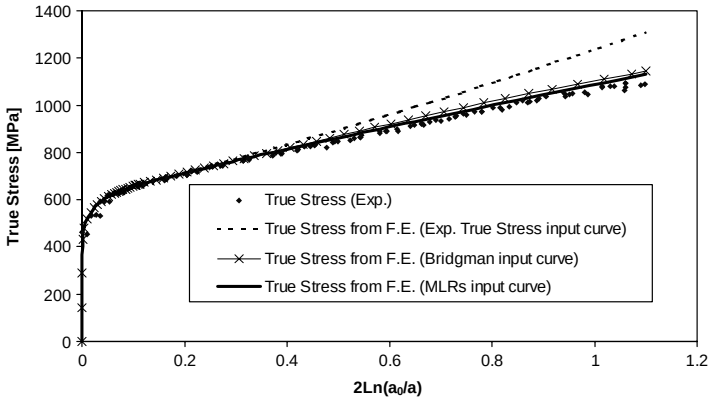

Fig. 9. Comparison between results from experiments and from three FE analyses.

5. Application and validation of the MLR model

The stress and strain distributions on the neck section are evaluated, for comparison purposes, at three post-necking levels approximately corresponding to logarithmic plastic strain values of 0.2 (slightly after the necking initiation), 0.6 (approximately at midpoint between necking and failure) and 1.1 (at incipient failure).

To calculate the distributions at a specific instant of the tensile test, the Bridgman method requires the experimental post-necking true curve (defined by the linear fitting of Table 1), the necking initiation strain ε_N, the initial and the current values of the cross-section radius a_0 and a respectively, and the current curvature radius R of the necking profile.

The MLR method requires the same experimental data listed above except the radius R, whose role (indicator of the necking perturbation level) is played by the material-independent polynomials of Figs. 2 and 3.

Figs. 10–15 show the stress and strain distributions across the neck section estimated, at each chosen stage of the tensile test, by the FEA, by the Bridgman method and by the MLR method proposed in this work.

It is evident that the MLR method gives much more realistic stress and strain distributions than the Bridgman method, also not considering the agreement with the FE distributions taken as reference. In fact, the MLR distributions do not exhibit the greater Bridgman approximations such as strain uniformity and perfect equivalence between radial and hoop stresses or radial and hoop strains. When the necking is just

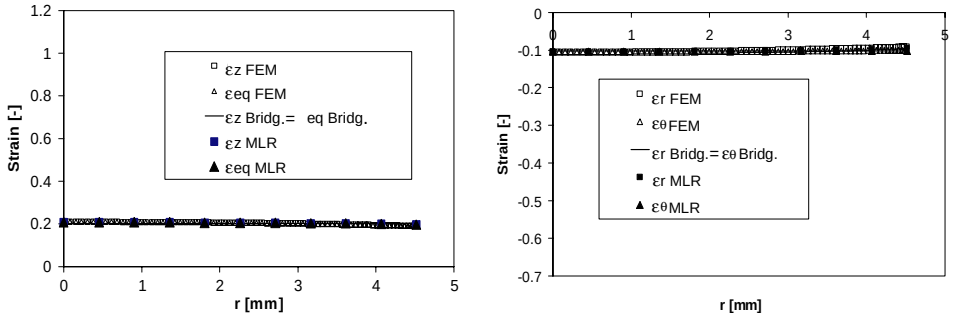

Fig. 10. Strain distributions on the neck at $2\,\mathrm{Ln}[a_0/a] = 0.2$.

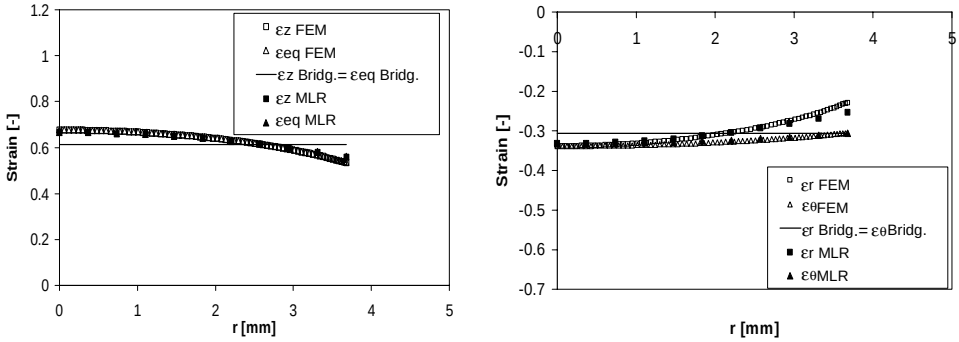

Fig. 11. Strain distributions on the neck at $2\,\mathrm{Ln}[a_0/a] = 0.6$.

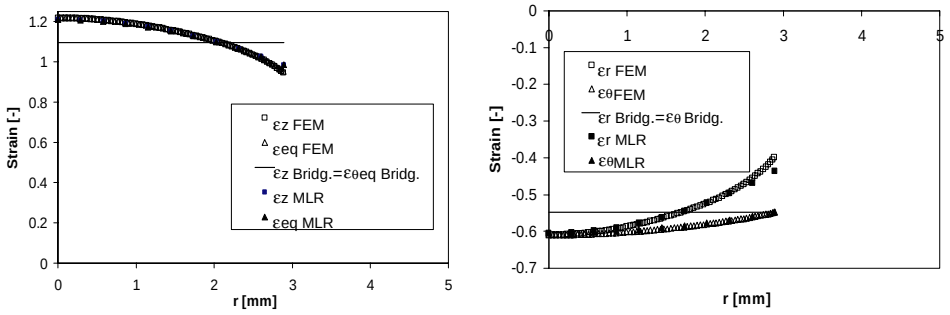

Fig. 12. Strain distributions on the neck at $2\,\mathrm{Ln}[a_0/a] = 1.1$.

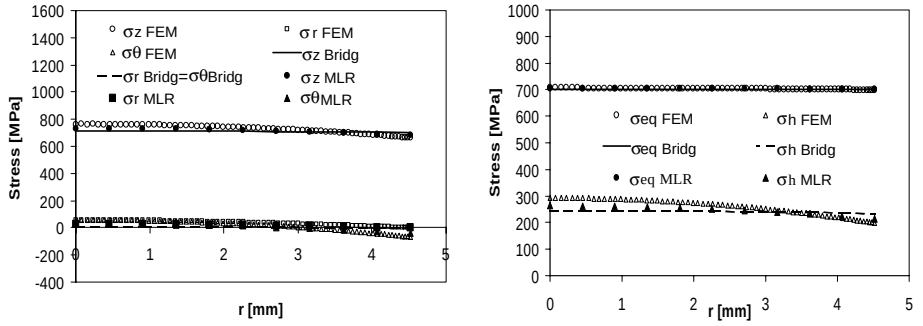

Fig. 13. Stress distributions on the neck at $2\,\mathrm{Ln}[a_0/a] = 0.2$.

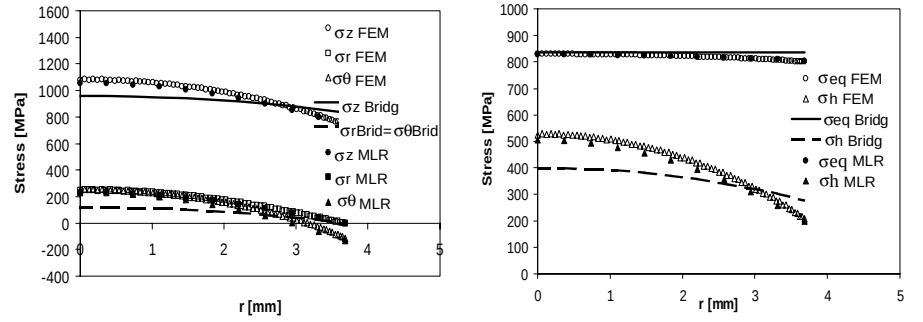

Fig. 14. Stress distributions on the neck at $2\,\mathrm{Ln}[a_0/a] = 0.6$.

initiated (Figs. 10 and 13) all the predictions by FE, Bridgman and MLR do not differ greatly each other, but under well developed necking conditions (Figs. 11, 12, 14 and 15) the discrepancies between the Bridgman distributions and the other two are definitely not negligible.

With regard to the strains it is possible to see that the values of ε_z are almost coincident with those of $\varepsilon_{\mathrm{eq}}$ as frequently assumed in the literature, on the contrary, ε_r and ε_θ coincide each other only on the neck section center (for $r = 0$) while, on the cross-section boundary ($r = a$), the radial strain evidently differs from the hoop strain as the theory suggests; according to the FE reference, the former has a value 27% lower than the latter at incipient failure.

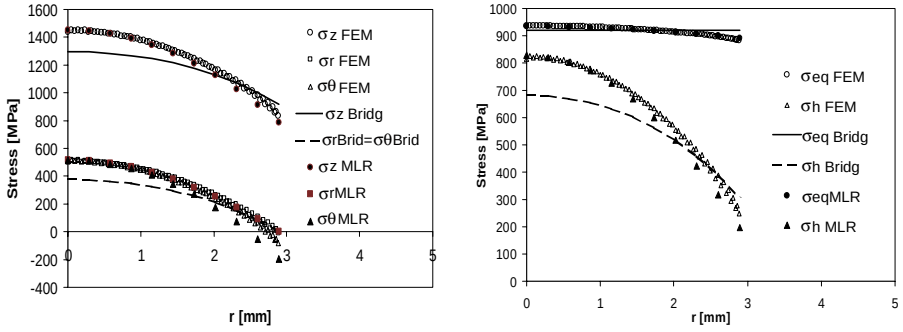

Fig. 15. Stress distributions on the neck at $2\,\mathrm{Ln}[a_0/a] = 1.1$.

The MLR method shows this feature with a certain approximation, in fact, at failure, for $r = a$, the maximum error in the MLR strains evaluation is close to 8%; however this error decreases rapidly while proceeding toward the neck center, where both the MLR radial and hoop strains are affected by a negligible error (<1%).

On the contrary, the maximum error in the Bridgman radial strain at failure is 37% for $r = a$ and 10% for $r = 0$.

Axial and equivalent strains calculated by the MLR method exhibit an error close to 3% on the outer surface and lower than 1% on the neck center while, in the same locations, the Bridgman method is affected by discrepancies close to 15% and 10% respectively.

Summarizing it is possible to say that the Bridgman method gives a considerable error on both the neck center and the neck boundary for all the strains calculated, the MLR method gives a negligible error in all the locations for all the strains except for the hoop strain on the outer surface, which is predicted to be 8% lower than the corresponding FEA-derived values.

A similar situation is observed with regard to the stresses, in fact the shapes of the Bridgman-evaluated stress distributions differ substantially from those of the FE reference in all the cases except for the equivalent stress, whose error is moderate and varies between 4% at the outer neck radius and slightly more than 1.5% on the neck center.

The error levels in the MLR-evaluated stresses are similar to those found in the corresponding strains, in fact the hoop stress σ_θ at the outer radius a is affected by the error in $\varepsilon_\theta(a)$ and results to be almost twice the value predicted by FEA, this being the maximum discrepancy of the entire set of MLR estimations.

Also the MLR hydrostatic stress on the outer neck radius is not very accurate, the error in this case being close to 20%, anyway, both the worst-accuracy MLR stresses, σ_θ and σ_H, on the neck center achieve error levels lower than 0.1%.

Table 3
Error of the stress and strain distributions on the neck

	Error with respect to FE results (%)								
	ε_z	ε_r	ε_θ	ε_eq	σ_z	σ_r	σ_θ	σ_eq	σ_H
Neck center, $r=0$									
Bridgman	9.9	9.3	9.3	9.9	10.6	27.3	27.3	1.5	17.7
MLR	0.7	0.8	0.8	0.7	<0.1	<0.1	<0.1	<0.1	<0.1
Neck boundary, $r=a$									
Bridgman	15.2	37	0	15.2	9.9	0	100	4.1	23.4
MLR	3.2	8.7	0	3.2	6.3	0	130	0.7	20.1

A summary of the errors from the Bridgman-evaluated and the MLR- evaluated stress and strain distributions at incipient failure is reported in Table 3, where in both cases the errors are calculated with respect to the FE results previously validated by comparison with experiments.

6. MLR model discussion

The basic idea behind the proposed model lies in a concept which was partially introduced also by Bridgman (1956), Hill (1950), Le Roy et al. (1981), Saie et al. (1982) and Zhang et al. (1999); that is the possibility that the necking, as well as many other instability phenomena, depends more on structural aspects such as load and boundary conditions rather than on the material properties.

An effort to cover this aspect can be found in the Bridgman work, where many values of the parameter, R/a, supposed to principally drive the necking perturbation, are plotted against the logarithmic plastic strain for different materials, suggesting the possibility that ratio could be material-independent. Nevertheless, the material independence does not strictly apply to this parameter as found in La Rosa et al. (2003), and as reported in the whole Bridgman work where is reported that "... consistent departures from the [average] curve [attempting to describe the common behavior of many materials] occur...".

Also the ratio $\sigma_{\mathrm{eqAvg}}/\sigma_{z\mathrm{Avg}}$, which in this paper is approximated by the function $\mathrm{MLR}_\sigma(\varepsilon_{\mathrm{eq}} - \varepsilon_{\mathrm{N}})$, was suspected to be material-independent by Bridgman, but the trends able to describe experimental data for different materials with an acceptable low scattering were not found in his work.

This was probably due to two causes; firstly, the R/a measurements were made by Bridgman after specimens unloading due to the lack of image analysis systems in those years, thus them were less accurate than nowadays standards; secondly, the variable with respect to which a material independence can be found, must take into account for each material's necking initiation strain ε_{N}: the reduced strain $\varepsilon_{\mathrm{eq}} - \varepsilon_{\mathrm{N}}$ used in this work is more suitable than simply $\varepsilon_{\mathrm{eq}}$, used by Bridgman, as a common variable for the post-necking histories of different material.

In the first part of this paper are reported the results of previous works in which FE analyses simulating tensile tests on cylindrical specimens, made of many different materials, allowed to gather interesting information about the stresses and strains on the neck section; these findings led to the definition of the MLR_σ polynomial approximating the ratio $\sigma_{\mathrm{eqAvg}}/\sigma_{z\mathrm{Avg}}$, suspected to be material-independent also by Bridgman; successively, a similar procedure led to the MLR_ε polynomial expressing the ratio $\varepsilon_{r\mathrm{Avg}}/\varepsilon_{\theta\mathrm{Avg}}$, firstly presented in this work; these two relationships, both material-independent, play the role which in the Bridgman work was played by the curve approximating, roughly, the R/a ratio for every material.

In order to derive the distributions of stress and strain on the neck section, both the axial plastic strain and the hydrostatic stress have been approximated by quadratic functions of the neck radial abscissa r.

With regard to the Bridgman method it is worth noting that its better performance is expressed in the calculation of the equivalent stress which, nevertheless being supposed to be uniform and independent from r, exhibits a degree of error quite lower than the other stresses or strains predicted by the same method. Clearly, the accuracy achievable with the Bridgman method strongly depends on the accuracy of the profiles curvature measurements.

From the viewpoint of the engineers who investigate metals properties, the MLR model can be used in two different ways to obtain as many families of data reflecting different material properties; the first and simpler use of the MLR method consists of correcting the experimental tensile true curve by multiplying the true-stress times the MLR_σ polynomial, this procedure leading to the material curve which expresses the equivalent von Mises stress as a function of the equivalent plastic strain; this means to characterize the material's elastoplastic behavior.

The second and more exhaustive use of the MLR method consists of solving the set of equations from (15)–(20) in order to calculate the stress and strain distributions across the necking section at every strain

level during the experimental tensile tests. This gives additional information such as the triaxiality development with the post-necking strain, other than a more local insight of the material behavior.

7. Conclusions

A result from previous works (La Rosa et al., 2003) was coupled with new data coming from many FE analyses, resulting in the estimated trends of two material-independent ratios between neck-averaged stresses and strains. This finding, consisting of two functions termed as MLR_σ and MLR_ε, already constitutes a tool for calculating the equivalent stress/equivalent strain curve in the post-necking phase of each material's life from the knowledge of just the experimental true curve. The accuracy of the material curve so obtained for a 20MnMoNi55 steel was verified by comparing the results from a FEA where this curve was used as input, with the results of experimental tests.

The same comparison was performed for two more FEA where respectively the Bridgman-corrected material curve and the not-corrected true curve were used to describe the material behavior. This multiple comparison between numerical and experimental data confirmed that the method proposed here for the material curve derivation is more accurate than that by Bridgman, other than definitely simpler to be used because requires no specific experimental data such as profile curvatures. Then, the stress and strain distributions on the neck section were derived by using the two MLR functions found before, together with two hypotheses regarding the shapes of the ε_z and σ_H distributions, both supposed to be quadratic with respect to the neck radial abscissa r.

This model was applied to the metal used in the experiments; the resulting distributions of stress and strain, together with those predicted by the Bridgman formulae, were compared with the distributions from the FEA taken as reference after the experimental validation.

The MLR-estimated distributions shown an high level of accuracy on the neck center, where an error lower than 1% was found for every principal stress and principal strain. On the outer boundary of the neck section the discrepancy between MLR and FE was more considerable, but here only two out of six principal stresses or strains shown an error higher than 10%.

In the same locations ($r = 0$ and $r = a$), the Bridgman predictions shown error levels considerably higher than those achieved by the proposed method, and also the overall shapes of the Bridgman distributions resulted to be less realistic than those predicted by the MLR model.

References

Alves, M., Jones, N., 1999. Influence of hydrostatic stress on failure of axisymmetric notched specimens. J. Mech. Phys. Solids 47, 643–667.

Becker, R., Tvergaard, V., et al., 1988. Void growth and failure in notched bars. J. Mech. Phys. Solids 36 (3), 317–351.

Bonora, N., 1997. A nonlinear CDM model for ductile failure. Eng. Fract. Mech. 58, 11–28.

Bridgman, P.W., 1956. Studies In Large Flow And Fracture. McGraw-Hill.

Chandrakanth, S., Pandey, P.C., 1995. An isotropic damage model for ductile material. Eng. Fract. Mech. 50, 457–465.

Earl, J.C., Brown, K.D., 1976. Distribution of stress and plastic strain in circumferentially notched tension specimens. Eng. Fract. Mech. 8, 599–611.

Hancock, J.W., Brown, D.K., 1983. On the role of strain and stress state in ductile failure. J. Mech. Phys. Solids 31, 1–24.

Hancock, J.W., Mackenzie, A.C., 1976. On the mechanisms of ductile failure in high strength steels subjected to multi-axial stress states. J. Mech. Phys. Solids 24, 147–169.

Hill, R., 1950. The Mathematical Theory of Plasticity. Oxford University Press.

La Rosa, G., Mirone, G., Risitano, A., 2000a. Numerical verification of the Bridgman model for notched and unnotched round specimens. In: Proc. Sixth International Conference on Damage and Fracture, May 2000, Montreal, Canada, pp. 553–563.

La Rosa, G., Mirone, G., Risitano, A., 2000b. Una nuova proposta numerico-sperimentale per la caratterizzazione elastoplastica. In: Proc. XV Italian National Congress IGF, Bari, Italy, pp. 361–371.

La Rosa, G., Mirone, G., Risitano, A., 2001. Effect of stress triaxiality corrected plastic flow on ductile damage evolution in the framework of continuum damage mechanics. Engineering Fracture Mechanics 68 (4), 417–434.

La Rosa, G., Mirone, G., Risitano, A., 2003. Post-necking elastoplastic characterization: degree of approximation in the Bridgman method and properties of the flow-stress/true-stress ratio. Met. Mat. Trans. A 34A (3), 615–624.

Lemaitre, J., 1988. Continuum damage mechanics: Parts I and II. J. Appl. Mech. 55, 59–72.

Le Roy, G., Embury, J.D., Edwards, G., Ashby, M.F., 1981. A model of ductile fracture based on the nucleation and growth of voids. Acta Metall. 29, 1509–1522.

Mackenzie, A.C., Hancock, J.W., Brown, D.K., 1977. On the influence of state of stress on ductile failure initiation in high strength steels. Eng. Fract. Mech. 9, 167–188.

Needleman, A., Tvergaard, V., 1984. An analysis of ductile rupture in notched bars. J. Mech. Phys. Solids 32 (6), 461–490.

Ragab, A.R., Saleh, A.R.Ch., 1999. Evaluation of constitutive models for voided solids. Int. J. Plast. 15, 1041–1065.

Saie, M., Pan, J., Needleman, A., 1982. Void nucleation effects on shear localization in porous plastic solids. Int. J. Fract. 19, 163–182.

Thomson, R.D., Hancock, J.W., 1984. Ductile failure by void nucleation, growth and coalescence. Int. J. Fract. 26, 99–112.

Wang, T.J., 1992. Unified CDM model and local criterion for ductile fracture—I. Unified CDM model for ductile fracture. Eng. Fract. Mech. 42, 177–183.

Zhang, Z.L., Hauge, M., Odegard, J., Thaulov, C., 1999. Determining material true stress–strain curve from tensile specimens with tensile cross-section. Int. J. Solids Struct. 36, 3497–3516.